Indian Journal of Pure & Applied Physics
Vol. 57, June 2019, pp. 385-399

Second law analysis of MHD Casson and Maxwell fluid flow over a permeable stretching sheet with homogenous heterogeneous reactions and variable heat source

Shalini Jain[a*] & Preeti Gupta[b]

[a]University of Rajasthan, Jaipur 302 004, India
[b]Manipal University Jaipur, Jaipur 303 007, India

Received 11 September 2018; accepted 01 March 2019

Entropy generation analysis of MHD Casson and Maxwell fluid flow over a stretching sheet with space and temperature dependent non-uniform heat source/sink with porous media has been explored. Using appropriate similarity transformations, governing equations have been changed into ODE's, and solved numerically using RK-fourth order method with shooting technique. The impact of pertinent parameters on velocity, temperature, entropy and Bejan number has been presented graphically. The skin friction and Nusselt number have been obtained and tabulated.

Keywords: Entropy analysis, Maxwell fluid, Casson fluid, Stretching sheet, Porous media, MHD

1 Introduction

The study of non-Newtonian fluids has attracted several researchers working in the field of geophysics, engineering, chemical and petroleum industry due to its wide applications, such as the extrusion of polymers fluids, exotic lubricants, animal bloods, solidification of liquid crystals and colloidal suspensions. Non-Newtonian fluids have been divided into three different types, namely rate type, differential type and integral type. Viscoelastic model is the simplest subclass of rate type fluids. Kumaran *et al.*[1] investigated Maxwell and Casson fluid flow over a sheet through MHD and cross diffusion. Ramesh *et al.*[2] investigated Maxwell stagnation point flow with permeable surface and nanoparticles. Ramesh and Gireesha[3] studied heat source/sink on Maxwell fluid past a sheet through nanoparticles and convective condition. Venkateswarlu and Satyanarayan[4] discussed MHD Maxwell fluid flow over a sheet with Soret and Dufour effect and joule heating. Madhu *et al*.[5] discussed unsteady Maxwell fluid flow through sheet with thermal radiation effect and MHD. Mukhopadhyay and Bhattacharya[6] studied unsteady Maxwell fluid flow through a sheet with chemical reaction. Aman *et al*.[7] studied heat transfer enhancement of CNTs Maxwell fluids with four kinds of molecular liquids. Aman *et al.*[8] discussed second order slip effect on flow of Maxwell nanofluid in a porous medium.

The Casson fluid has an extensive variety of applications pertaining to industry, science and engineering, specifically in the process of crude oil extraction from petroleum products. Mahanthesh *et al.*[9] discussed Margoni convection in Casson fluid flow through infinite disk through cross diffusion and exponentially heat source. Jain and Choudhary[10] discussed flow of Casson fluid past a wedge through heat source, MHD, thermophoretic effect and Dufour-Soret effect. Gopal *et al.*[11] studied Joule's and viscous dissipation on Casson fluid flow with inclined magnetic field over a chemical reacting stretching sheet. Raju and Sandeep[12] studied Casson fluid over a moving geometry through MHD and heat source/sink. Ullah *et al.*[13] discussed Casson fluid through a nonlinearly sheet through slip and porous media. Qayyum *et al.*[14] investigated fluid-solid interface in squeezing the flow of MHD Casson fluid with porous media.

Srinivas *et al.*[15] studied pulsating flow of Casson fluid in a porous channel through applied magnetic field, chemical reaction and thermal radiation. Yousif *et al.*[16] discussed 3-dimensional flow of MHD Casson fluid through porous linearly sheet. Ariel *et al*.[17] studied boundary layer flow due to sheet through partial sleep. Ferdows *et al.*[18] discussed chemical reaction effect on boundary layer flow over a linearly

*Corresponding author (E-mail: drshalinijainshah@gmail.com)

sheet. Haque *et al.*[19] studied stability analysis and numerical simulation on free convection unsteady flow with porous media in a rotating system in the presence of induced magnetic field.

Most of the chemical reacting system with homogeneous-heterogeneous reactions are used in combustion, biochemical system, catalysis, fog formation and dispersion, ceramics and polymer production, food processing and are also involved in the consumption and creation of reactant species. Merkin[20] analyzed the catalyst surface, heterogeneous reaction and homogenous reaction for cubic autocatalysis, and introduced that surface reaction is dominant near the surface. Bachok *et al.* [21] studied stagnation flow past a sheet with homogenous heterogeneous reactions. Many researchers Kameswaran *et al.*[22], Malik *et al.*[23] and Sheikh and Abbas[24] discussed heat transfer through homogenous-heterogeneous reactions.

According to thermodynamics second law, flow and heat transfer procedures undergo fluctuations that are irreversible caused by energy damages during the processes. Such impacts cannot be entirely eliminated from system, as a result system losses energy. In thermodynamics, irreversibility is measured by entropy generation rate. Bejan[25] investigated entropy generation analysis. Shateyi *et al.*[26] used spectral relaxation method for second law analysis of Maxwell fluid through MHD. Ahmad *et al.*[27] discussed thermodynamics second law effect of double diffusive Casson fluid flow through nonlinear stretching sheet through slip condition. Qing *et al.*[28] studied entropy analysis in Casson MHD nanofluid flow past a porous sheet. Selvi *et al.*[29] discussed thermodynamic effect on Casson MHD nanofluid flow in a vertical porous through stretching walls. Qasim *et al.*[30] studied entropy analysis in the flow of methanol-based nanofluid in a wavy channel.

Many researchers Bhatti *et al.*[31], Jamalabadi *et al.*[32], Srinivasacharya and Bindu[33], Jangili *et al.*[34], Baag et al.[35], Rehman et al.[36], Zhu *et al.*[37], Srinivas and Murthy[38], Kareem *et al.*[39], and Khan *et al.*[40] discussed entropy generation analysis of non-Newtonian flow of fluid through different geometries. Jain *et al.*[41] studied Second law analysis of couette flow with thermal boundary conditions and porous medium.

The aim of this study is to analyze entropy generation of an incompressible Maxwell and Casson fluid flow past a sheet with homogenous heterogeneous reaction through space and temperature dependent non-uniform heat source/sink and porous media. Thus, fluid velocity, concentration, temperature distribution, entropy and Bejan number have been analyzed and presented through figures.

2 Mathematical Formulation

Entropy analysis of a steady incompressible MHD flow of both Casson and Maxwell fluid past a stretching sheet placed along x-axis and perpendicular to y-axis with porous media and space and temperature dependent non-uniform heat source/sink has been considered. Flow of fluid is generated due to stretching of sheet $U_W = \omega x$, by using two equal and opposite forces and T_W is fluid temperature near the boundary. We have assumed that underline part of stretching sheet is occupied with hot fluid.

Homogeneous and heterogeneous equations with two chemical species A and B has also been considered. The cubic catalysis in homogenous reaction is given as:

$$A + 2B \to 3B, \text{ rate} = k_c ab^2, \quad \ldots(1)$$

while catalyst surface on heterogeneous reaction is given as:

$$A \to B, \text{ rate} = k_5 a, \quad \ldots(2)$$

where, k_c and k_s are rate constants and a and b are concentrations of chemical species A and B. Schematic diagram shown in figure 1.

The flow equations including the continuity, homogenous and heterogeneous equation, momentum and energy equations can be written as:

$$\frac{\partial u}{\partial x} + \frac{\partial v}{\partial y} = 0, \quad \ldots(3)$$

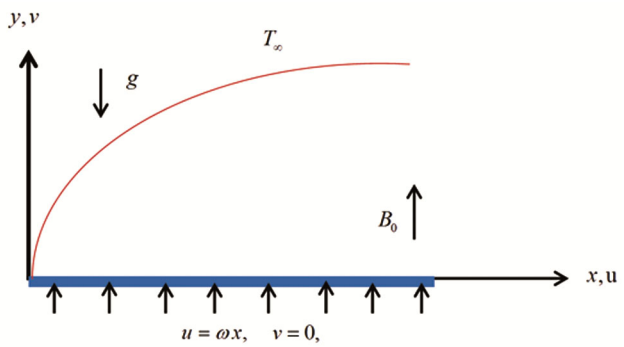

Fig. 1 — Schematic diagram.

$$u\frac{\partial u}{\partial x}+v\frac{\partial u}{\partial y}=\upsilon\left(1+\frac{1}{\beta}\right)\frac{\partial^2 u}{\partial y^2}--\frac{\sigma {B_0}^2}{\rho}\left(\lambda_v v\frac{\partial u}{\partial y}+u\right)$$
$$\lambda_v\left(u^2\frac{\partial^2 u}{\partial x^2}+v^2\frac{\partial^2 v}{\partial x^2}+2uv\frac{\partial^2 u}{\partial x\partial y}\right)-\frac{\upsilon}{k_p}u, \quad \ldots (4)$$

$$u\frac{\partial a}{\partial x}+v\frac{\partial a}{\partial y}=D_A\frac{\partial^2 a}{\partial y^2}-k_c ab^2, \quad \ldots (5)$$

$$u\frac{\partial b}{\partial x}+v\frac{\partial b}{\partial y}=D_B\frac{\partial^2 b}{\partial y^2}+k_c ab^2, \quad \ldots (6)$$

$$u\frac{\partial T}{\partial x}+v\frac{\partial T}{\partial y}=\alpha\left(\frac{\partial^2 T}{\partial y^2}\right)+\frac{\mu}{\rho c_p}\left(1+\frac{1}{\beta}\right)\left(\frac{\partial u}{\partial y}\right)^2+\frac{q'''}{\rho c_p}, \quad \ldots (7)$$

Under the boundary conditions at stretching sheet:

$$\text{at } y=0,\ u=U_w=\omega \text{x},\ v=0,\ D_A\frac{\partial a}{\partial y}=k_s a,$$
$$D_B\frac{\partial b}{\partial y}=-k_s a,\ -k\frac{\partial T}{\partial y}=h_f\left(T_W-T\right),$$
$$\text{at } y\to\infty,\ u\to 0,\ a\to a_0,\ b\to 0,\ T\to T_\infty, \quad \ldots(8)$$

here, (u,v) are the velocity component in the (x, y) direction respectively, ρ is the density, μ is the dynamic viscosity, D_A and D_B are diffusion coefficients, c_p is the specific heat. T,T_W and T_∞ are the fluid temperature, surface temperature and ambient temperature. The PDE's have been changed into ODE's by using following transformations:

$$\eta=\left(\frac{\omega}{\upsilon}\right)^{\frac{1}{2}}\text{y},\ \psi=(\omega\upsilon)^{\frac{1}{2}}xf(\eta),\ a=a_0\varphi(\eta),$$
$$b=a_0 h(\eta),\ \theta(\eta)=\frac{T-T_\infty}{T_W-T_\infty}, \quad \ldots (9)$$

where, ψ is the stream function to describe the velocity components as:

$$u=\frac{\partial\psi}{\partial y}\ \text{and}\ v=-\frac{\partial\psi}{\partial x}$$

The space and temperature dependent non-uniform heat source/sink is given as follows:

$$q'''=\frac{kU_w}{x\upsilon}\left\{A^*\left(T_w-T_\infty\right)f'(\eta)+B^*\left(T-T_\infty\right)\right\}, \quad \ldots (10)$$

where, υ is the kinematic fluid viscosity, A^* and B^* are the space and the temperature dependent heat source/sink parameter and k is thermal conductivity.

Equation (3) is identically satisfied, now substituting Eq. (9) into Eqs. (4)-(7) we get the following nonlinear equations:

$$\left(1+\frac{1}{\beta}-\delta_m f^2\right)f'''-f'^2+\left(1+M\delta_m\right)ff''+2\delta_m ff'f''-\left(M+K\right)f'=0, \quad \ldots (11)$$

$$\frac{1}{Sc}\varphi''+f\varphi'-k_1\varphi h^2=0, \quad \ldots (12)$$

$$\frac{\delta_1}{Sc}\text{h}''+f\,\text{h}'+k_1\varphi h^2=0, \quad \ldots (13)$$

$$\theta''+\Pr\left[f\theta'+\left(1+\frac{1}{\beta}\right)Ecf''^2\right]+(\text{A}^*f'+B^*\theta)=0, \quad \ldots (14)$$

using Eq. (9) in Eq. (8), the related boundary conditions become:

$$\text{at } \eta=0,\ f'(\eta)=1,\ f(\eta)=0,\ \varphi'(0)=k_2\varphi(0),$$
$$\delta_1 h'(0)=-k_2\varphi(0),\ \theta(\eta)=1+\left(\frac{1}{Bi}\right)\theta',$$
$$\text{at } \eta\to\infty,\ f'(\eta)\to 0,\ \varphi(\infty)\to 1,\ h(\infty)\to 0,$$
$$\theta(\eta)\to 0, \quad \ldots (15)$$

Also, assuming that both the chemical species have equal diffusion coefficients D_A and D_B. i.e. $\delta_1=1$, thus

$$\varphi(\eta)+h(\eta)=1 \quad \ldots (16)$$

Now Eqs (12) and (13) become:

$$\frac{1}{Sc}\varphi''+f\varphi'-k_1\varphi(1-\varphi)^2=0, \quad \ldots (17)$$

under the boundary conditions

$$\varphi'(0)=k_2\varphi(0),\ \varphi(\infty)\to 1, \quad \ldots (18)$$

where, $\delta_m = \lambda_v \omega,$ is the viscoelastic parameter, $M = \frac{\sigma B_0^{\,2}}{\omega\rho},$ is the magnetic parameter, $K = \frac{\upsilon}{k_p \omega},$ is the permeability parameter, $Sc = \frac{\upsilon_f}{D_A},$ is the Schmidt number, $\delta_1 = \frac{D_B}{D_A},$ is the ratio of diffusion coefficient, $k_1 = \frac{k_c a_0^{\,2}}{\omega},$ and $k_2 = \frac{k_S}{D_A}\sqrt{\frac{\upsilon}{\omega}},$ are the homogeneous and heterogeneous strength, $\Pr = \frac{\mu C_p}{k},$ is the Prandtl number, $Ec = \frac{U_w^{\,2}}{c_p\left(T_w - T_\infty\right)},$ is the Eckert number.

The study has been done for following two cases:

Case-I Maxwell fluid model

$\beta = \infty$ and $\delta_m = 0.5.$

Case-II Casson fluid model

$\delta_m = 0$ and $\beta = 1.0.$

The Skin friction coefficient $C_f,$ and the Nusselt number for heat transfer $Nu_x,$ is given as follows.

$$C_f = \frac{\tau_w}{\rho U_w^{\,2}}, \qquad Nu_x = \frac{x q_w}{k(\mathrm{T}_w - \mathrm{T}_\infty)},$$

here, the wall shear stress $\tau_w,$ and wall heat transfer q_w are as follows

$$\tau_w = \mu\left(1+\delta_m\right)\left(\frac{\partial u}{\partial y}\right)_{y=0}, \quad q_w = -k\left(\frac{\partial T}{\partial y}\right)_{y=0},$$

By using similarity transformation, we obtain dimensionless parameters

$$\mathrm{Re}^{\frac{1}{2}} C_f = \left(1+\delta_m\right)\left(1+\frac{1}{\beta}\right) f''(0),$$

$$\mathrm{Re}^{\frac{-1}{2}} Nu_x = -\theta'(0),$$

3 Method of Solution

In present study, Eqs (11), (14) and (17) under the boundary conditions (15) and (18) solved numerically by RK-4 method with shooting technique. The RK method needs a finite domain $0 \le \eta \le \eta_\infty.$ In this investigation, we have taken $\eta_\infty = 10.$ The BVP is transformed into IVP, are defined as:

Assuming

$f = f1, f' = f2, f'' = f3,\ \varphi = f4, \varphi' = f5,$
$\theta = f6, \theta' = f7,$

$$f_3' = \frac{1}{\left(1+\frac{1}{\beta}-\delta_m f_1^2\right)}\left\{\begin{matrix} f_2^{\,2} - \left(1+M\delta_m\right) f_1 f_3 - \\ 2\delta_m f_1 f_2 f_3 + \left(M+K\right) f_2 \end{matrix}\right\},$$

$$f_5' = -Sc\left\{f_1 f_5 - k_1 f_4 \left(1-f_4\right)^2\right\},$$

$$f_7' = -\Pr\left[f_1 f_7 + \left(1+\frac{1}{\beta}\right) Ec f_3^{\,2}\right] - (\mathrm{A}^* f_2 + B^* f_6),$$

Under the boundary condition

at $\eta = 0,\ f_2 = 1,\ f_1 = 0,\ f_5 = k_2 f_4,\ f_6 = 1 + \left(\frac{1}{Bi}\right) f_7,$

at $\eta \to \infty,\ f_2 \to 0,\ f_4 \to 1,\ f_6 \to 0,$

$$f_3(0) = r_1, f_5(0) = r_2, f_7(0) = r_3,$$

where, r_1, r_2, r_3 are the initial guesses.

We take the series of values for $f''(0),$ $\varphi'(0)$ and $\theta'(0)$ and apply fourth order Runge-Kutta method with step size $\Delta\eta = 0.01.$ The above process is repeated until we find the converged results within a tolerance limit of 10^{-5}.

4 Entropy Analysis

The local volumetric entropy equation rate of the Casson and Maxwell fluid with porous medium is written as:

$$S'''_{gen} = \frac{k^*}{T_\infty^{\,2}}\left(\frac{\partial T}{\partial y}\right)^2 + \frac{\mu}{T_\infty}\left(1+\frac{1}{\beta}\right)\left(\frac{\partial u}{\partial y}\right)^2 + \left(\frac{\sigma B_0^{\,2}}{T_\infty} + \frac{\mu}{k_p T_\infty}\right) u^2 \qquad \ldots (19)$$

The non-dimensional form of characteristic entropy generation rate is:

$$S'''_0 = \frac{k^*\left(T_w - T_\infty\right)^2}{T_\infty{}^2 x^2}, \quad \ldots (20)$$

hence, the entropy generation parameter is:

$$N_G = \frac{S'''_{gen}}{S'''_0}, \quad \ldots (21)$$

On using Eqs (19) and (20) in Eq. (21), reduces to the following equation:

$$N_G = \mathrm{Re}_L\,\theta'^2 + \left(\frac{\mathrm{Re}_L\,Br}{\Omega}\right)\left(1+\frac{1}{\beta}\right)f''^2 + \left(\frac{\mathrm{Re}_L\,Br}{\Omega}\right)(M+K)\,f'^2, \quad \ldots (22)$$

where, $\mathrm{Re}_L, Br, \Omega$ denotes the Reynolds number, Brinkman number, dimensionless temperature difference respectively. These parameters are:

$$Br = \frac{\mu\omega^2 x^2}{\mathrm{k}^*\left(T_W - T_\infty\right)},\ \Omega = \frac{T_W - T_\infty}{T_\infty},\ \mathrm{Re}_L = \frac{\omega x^2}{\upsilon}, \quad \ldots (23)$$

For calculating irreversibility distribution, the Bejan number is presented, which is ratio of heat transfer irreversibility to entropy generation number.

$$Be = \frac{\mathrm{Re}_L\,\theta'^2}{\left\{\mathrm{Re}_L\,\theta'^2 + \left(\frac{\mathrm{Re}_L\,Br}{\Omega}\right)\left(1+\frac{1}{\beta}\right)f''^2 + \left(\frac{\mathrm{Re}_L\,Br}{\Omega}\right)(M+K)\,f'^2\right\}}, \quad \ldots (24)$$

5 Validation of Present Study

Table 1 shows a comparison of numerical values of $\theta'(0)$ obtained in the present investigation considering

Table 1 — Comparison of the values of $-\theta'(0)$ with that of Chen *et al.*, Zaimi *et al.* and Naramgari *et al.* when $K = 0, \delta_m = 0,1 / \mathrm{Bi} = 0, Ec = 0,1 / \beta = 0, \mathrm{M} = 0, \mathrm{A}^* = 0, \mathrm{B}^* = 0.$

Pr	Chen[33] $-\theta'(0)$	Zaimi *et al.* $-\theta'(0)$	Naramgari *et al.*[31] $-\theta'(0)$	Present study $-\theta'(0)$
0.72	0.46315	0.463145	0.463146	0.463592894
1	0.58199	0.581977	0.581979	0.582012437
3	1.16523	1.165246	1.165249	1.165248737
7	1.89537	1.895403	1.895406	1.895417239
10	2.30796	2.308004	2.308008	2.308031964

$K = 0, \delta_m = 0,1 / \mathrm{Bi} = 0, Ec = 0,1 / \beta = 0, \mathrm{M} = 0,$
$\mathrm{A}^* = 0, \mathrm{B}^* = 0$

with the results obtained by Chen *et al.*[33] , Zaimi *et al.* [32] and Naramgari *et al.*[31] It is noted that the results obtained are in excellent agreement with literature available.

6 Results and Discussion

The numerical results have been found for entropy analysis of Casson and Maxwell fluid flow through stretching sheet and shown graphically. Effect of pertinent parameters like δ_m is the Maxwell parameter, M is the magnetic parameter, β is the Casson parameter, K is the permeability parameter, A* and B* are space and temperature dependent heat source/sink parameter, Sc is the Schmidt number, k_1 and k_2 are the homogeneous and heterogeneous strength, Pr is the Prandtl number, Ec is the Eckert number, Bi is the Biot number, Re is the Reynolds number, Br is the Brinkman number, Ω is the dimensionless temperature difference on velocity, temperature, concentration and entropy are presented through graphs.

$K = 0.1, \delta_m = 0.5, \beta = 1, \mathrm{M} = 1, \mathrm{A}^* = 0.2, \mathrm{B}^* = 0.2,$
$\mathrm{Sc} = 0.7, \mathrm{k1} = 0.2, \mathrm{k\,2} = 0.1, \mathrm{Bi} = 0.5, \mathrm{Pr} = 2.5,$
$Ec = 0.1, Br = 1, \Omega = 1, \mathrm{Re} = 1$

Table 2 shows that the influences of different non-dimensional parameters on skin friction coefficient $\left(\mathrm{Re}^{\frac{1}{2}} C_f\right)$. Skin friction coefficient increases with enhancing value of β while reverse impact shows with increasing value of $\mathrm{K}, \delta_m, \mathrm{M}$. The influences of different non-dimensional parameters on Nusselt number. Temperature profile enhances with increasing values of $\mathrm{Pr}, \mathrm{Bi},$ while reverse impact shows with increasing value of $K, \delta_m, \beta, \mathrm{M}, \mathrm{A}^*, B^*, Ec.$

Figures 2 and 3 present the consequences of Casson parameter and magnetic parameter on the velocity distribution. In Fig. 2 velocity decreases with increasing value of Casson parameter. Physically, reduced yield stress suppresses the velocity. In Fig. 3 enhancing value of magnetic parameter decreases the flow field. Physically, increasing the magnetic parameter produced the Lorentz force (resistive force) to the flow. This force has a tendency to suppress the velocity field. It has also been observed that boundary

Table 2 — Variation of skin friction and Nusselt number for Casson and Maxwell fluid

K	δ_m	β	M	A^*	B^*	Pr	Ec	Bi	$\frac{1}{\mathrm{Re}^{\frac{1}{2}}} C_f$	$\frac{-1}{\mathrm{Re}^{\frac{1}{2}}} Nu_x$
0.1	0.5	1.0	1.0	0.2	0.2	1.5	0.1	1	-3.381001665	0.155291876
0.5									-3.635364341	0.133425676
1.0									-3.930884009	0.104813400
	0.0								-2.049390403	0.190558175
	0.5								-3.381001665	0.155291876
	1.0								-4.894221271	0.113219852
		1.0							-3.381001665	0.155291876
		2.0							-2.928004302	0.133633396
		3.0							-2.760533217	0.119167078
			1.0						-3.381001665	0.155291876
			2.0						-4.087541182	0.079068237
			3.0						-4.688832185	-0.017490248
				0.1					-3.381000280	0.202547045
				0.2					-3.381001665	0.155291876
				0.3					-3.381004320	0.108037014
					0.1				-3.381000280	0.215684386
					0.2				-3.381001665	0.155291876
					0.3				-3.380998018	0.061128160
						1.0			-3.381016173	-0.110547922
						1.5			-3.381001665	0.155291876
						2.0			-3.381026035	0.235272106
							0.1		-3.381001665	0.155291876
							0.2		-3.381001665	0.053065122
							0.3		-3.380998018	-0.049159745
								1.0	-3.381001665	0.155291876
								2.0	-3.381000278	0.188464717
								3.0	-3.381000278	0.202912957

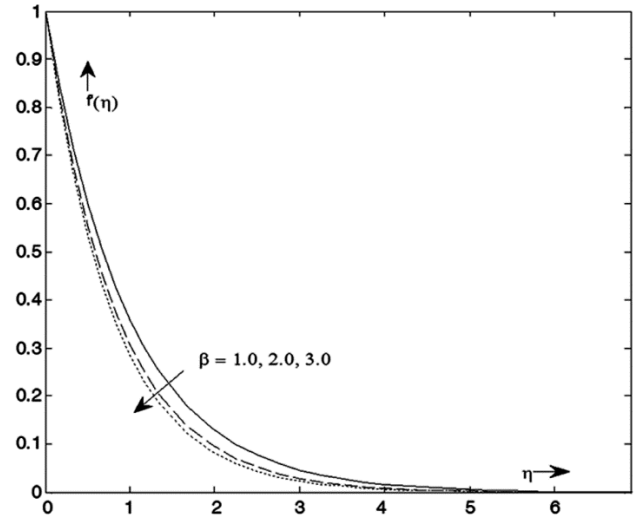

Fig. 2 — Effect of variation of the Casson parameter on velocity profile when $K = 0.1, \delta_m = 0.5, \mathrm{M} = 1.$

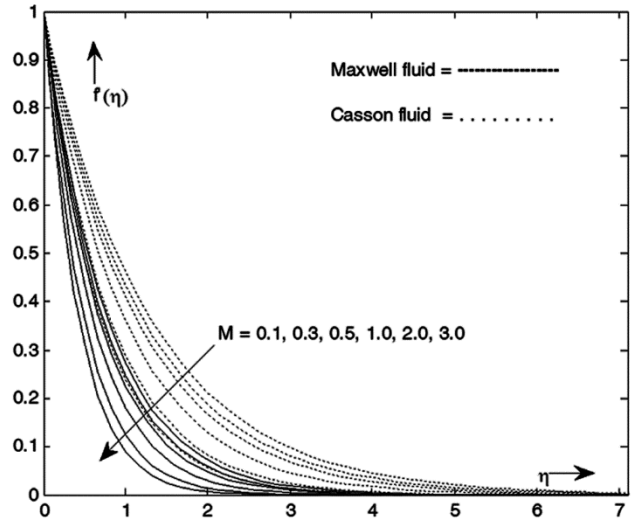

Fig. 3 — Effect of variation of the magnetic parameter on velocity profile when $K = 0.1$

layer flow of Maxwell fluid is more influenced by Lorentz force as compared with Casson fluid.

Figures 4 and 5 depict the impacts of permeability parameter and Maxwell fluid parameter on fluid velocity distribution. The increasing values of permeability and Maxwell parameter will lead to decline fluid velocity profile across the boundary layer flow. Physically, in viscoelastic fluid the delay

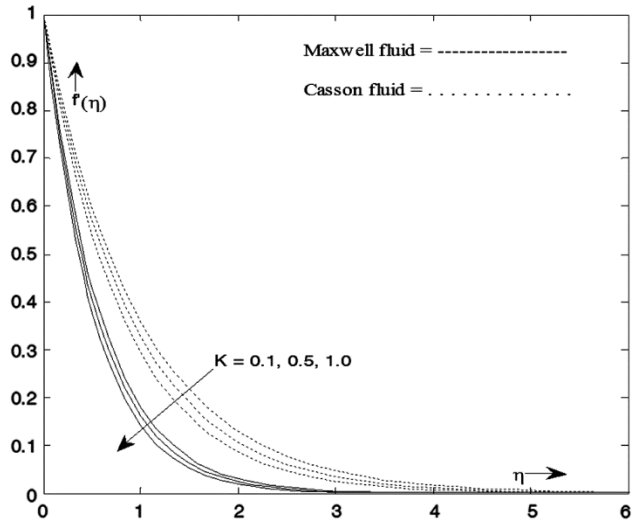

Fig. 4 — Effect of variation of the permeability parameter on velocity profile when $M = 1$.

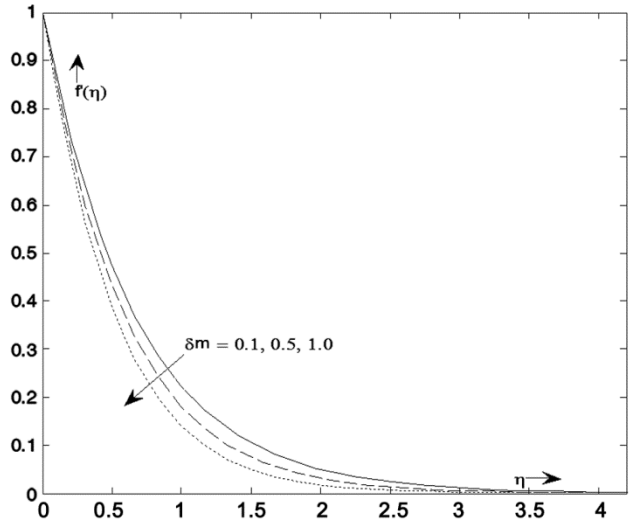

Fig. 5 — Effect of variation of the Maxwell parameter on velocity profile when $K = 0.1, \beta = 1, M = 1$.

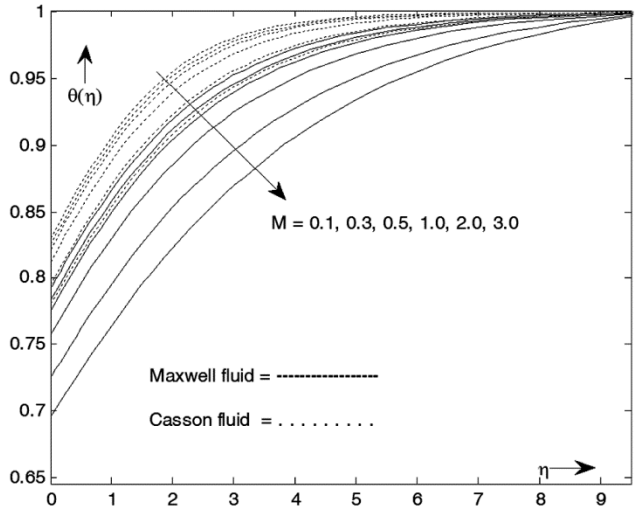

Fig. 6 — Effect of variation of the magnetic parameter on concentration profile when $K = 0.1, Sc = 0.7, k1 = 0.2, k2 = 0.1$.

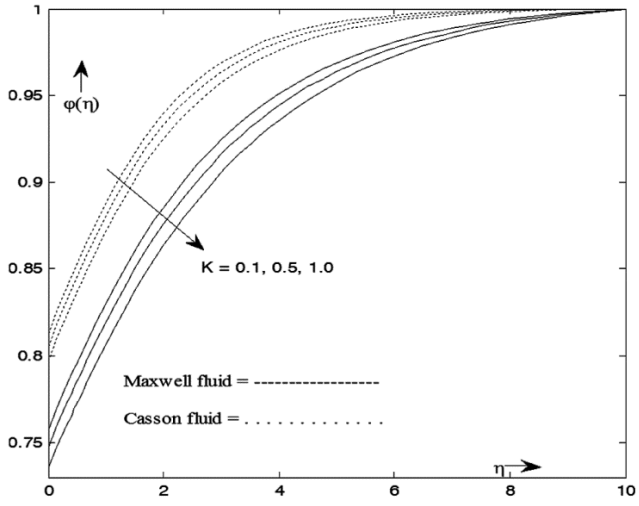

Fig. 7 — Effect of variation of the permeability parameter on concentration profile when $M = 1, Sc = 0.7, k1 = 0.2, k2 = 0.1$.

response of strain layer by layer, reason behind this relaxation behavior. So the Maxwell parameter is contributed to decay the velocity profile in shear flow. Figures 6 and 7 represent the influences of magnetic parameter and permeability parameter on concentration profile. It is observed that the concentration decreases with a rise in magnetic parameter and permeability parameter.

Figure 8 describes that the concentration distribution is a declining function of homogenous reaction parameter for both the non-Newtonian fluids. In fact, higher values of homogeneous parameter correspond to larger chemical reaction which consequently diminishes the concentration profile. The difference in concentration profile for different values of heterogeneous parameter is presented in Fig. 9. The solutal boundary layer thickness declines for different fluids. Because heterogeneous parameter has an inverse relation with mass diffusivity. Figure 10 illustrates the performance of Schmidt number on concentration distribution. It is observed that for enhancing values of Schmidt number the concentration profile increases because the Schmidt

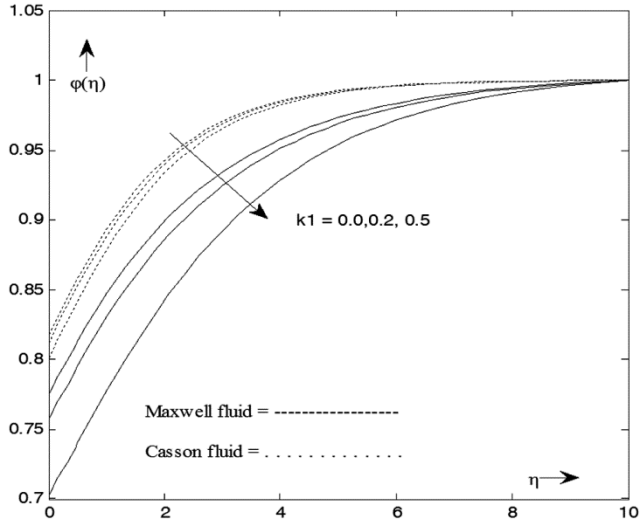

Fig. 8 — Effect of variation of the homogeneous reaction parameter on concentration profile when $K = 0.1, \mathrm{M} = 1, \mathrm{Sc} = 0.7, \mathrm{k}2 = 0.1$.

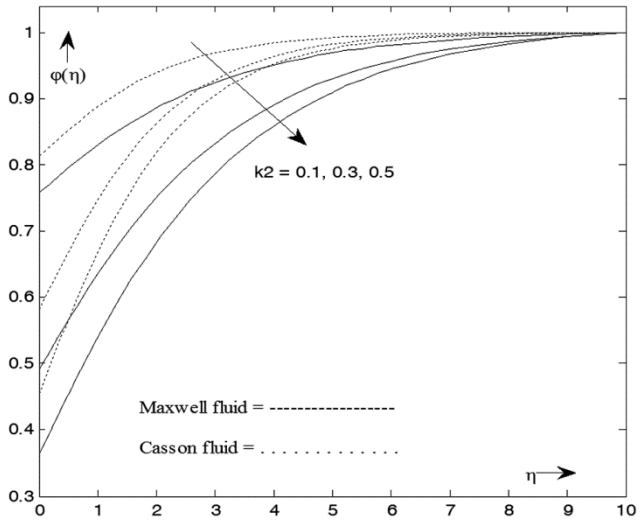

Fig. 9 — Effect of variation of the heterogeneous reaction parameter on concentration profile when $K = 0.1, \mathrm{M} = 1, \mathrm{Sc} = 0.7, \mathrm{k}1 = 0.2$.

number is the ratio of momentum diffusivity to mass diffusivity. So by enhancing Schmidt number minimum mass diffusivity takes place, causing concentration of the fluid to increase. Figure 11 indicates the influence of permeability parameter on temperature profile. Permeability parameter increases with increasing values of temperature distribution.

Figures 12 and 13 illustrate the influence of magnetic and Biot number on temperature distribution. Magnetic parameter and Biot number on the temperature distribution increase with increasing values of temperature profile. Effect of magnetic

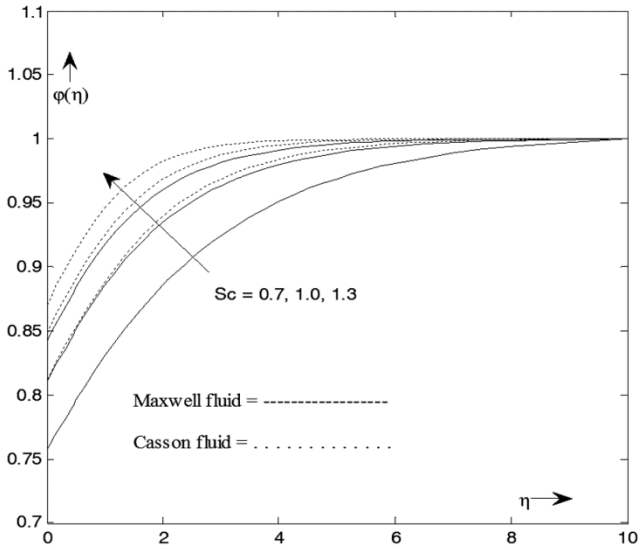

Fig. 10 — Effect of variation of the Schmidt number on concentration profile when $K = 0.1, \mathrm{M} = 1, \mathrm{k}1 = 0.2, \mathrm{k}2 = 0.1$.

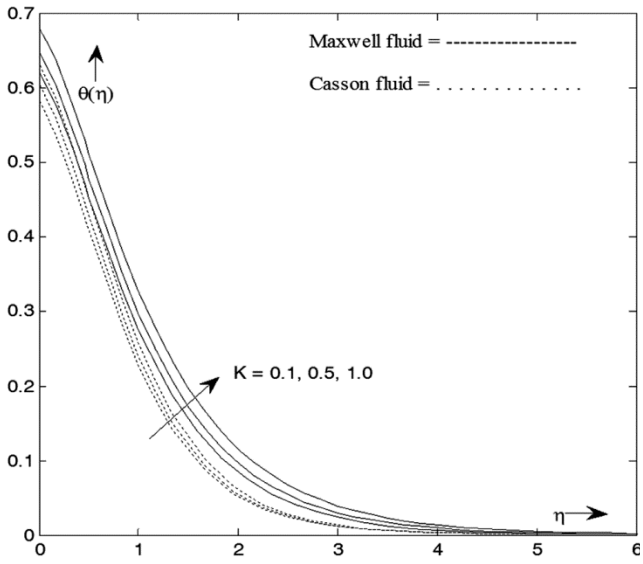

Fig. 11 — Effect of variation of the permeability parameter on temperature profile when
$\mathrm{M} = 1, \mathrm{A}^* = 0.2, \mathrm{B}^* = 0.2, \mathrm{Sc} = 0.7, \mathrm{k}1 = 0.2, \mathrm{k}2 = 0.1, \mathrm{Bi} = 0.5,$
$\mathrm{Pr} = 2.5, Ec = 0.1$.

parameter is predicted to enhance the wall temperature gradient. Due to this higher temperature gradient at the wall, hence, higher wall heat transfer. The magnetic parameter is not directly performing in energy equation, but it indirectly affects on temperature profile through changes in velocity profile. In Fig.13 effect of Biot number is higher on Maxwell flow. It may happen due to decreased viscosity nature for enhancing values of Biot number.

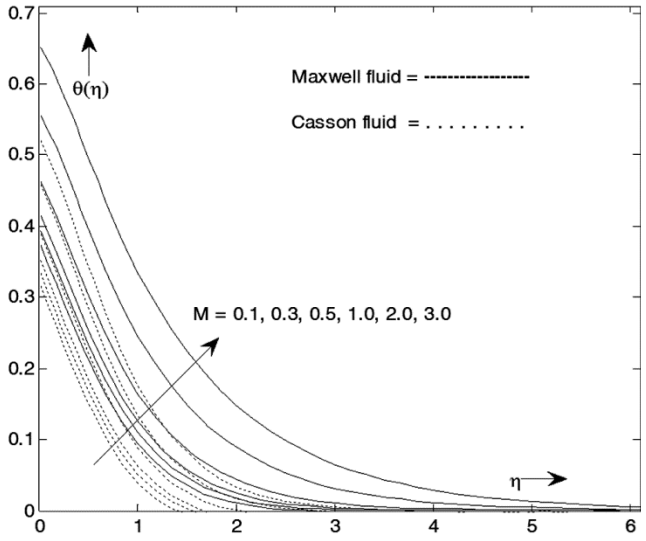

Fig. 12 — Effect of variation of the magnetic parameter on temperature profile when
$K = 0.1, A^* = 0.2, B^* = 0.2, Sc = 0.7, k1 = 0.2, k2 = 0.1, Bi = 0.5,$
$Pr = 2.5, Ec = 0.1.$

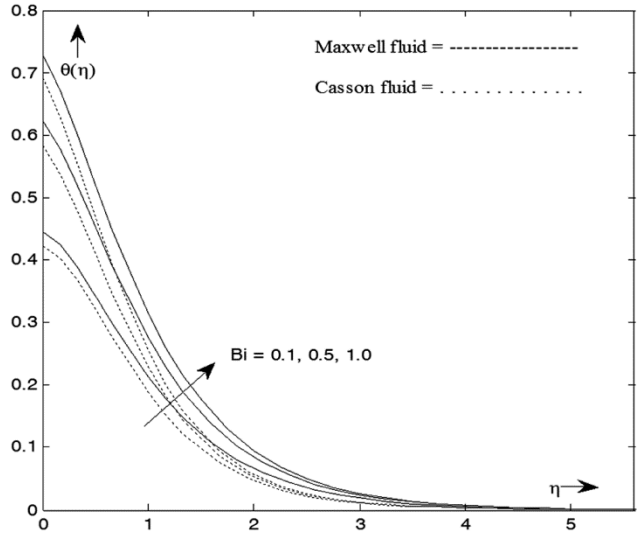

Fig. 13 — Effect of variation of the Biot number on temperature profile when
$K = 0.1, M = 1, A^* = 0.2, B^* = 0.2, Sc = 0.7, k1 = 0.2, k2 = 0.1,$
$Pr = 2.5, Ec = 0.1.$

Physically, enhancing Biot number increases the temperature difference. This leads to enhance the temperature distribution of the flow.

Figures 14 and 15 show the influence of space and temperature dependent heat source/sink parameter. The space and temperature dependent heat source/sink parameter enhances with enhancing values of

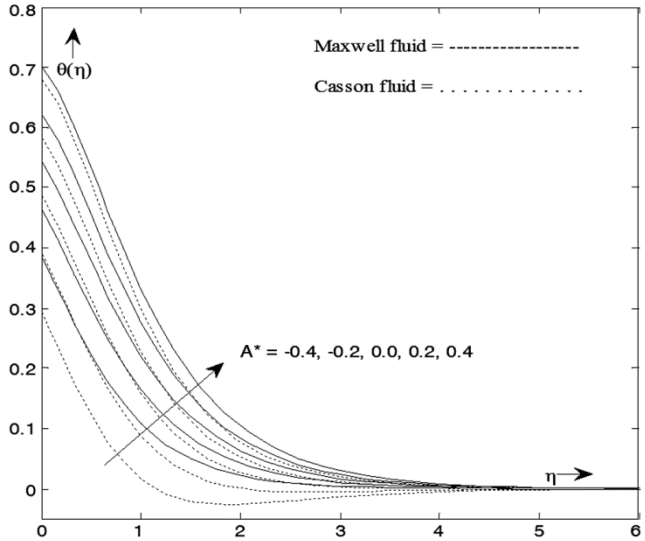

Fig. 14 — Effect of the space dependent heat source/sink parameter on temperature when
$K = 0.1, M = 1, B^* = 0.2, Sc = 0.7, k1 = 0.2, k2 = 0.1, Bi = 0.5,$
$Pr = 2.5, Ec = 0.1.$

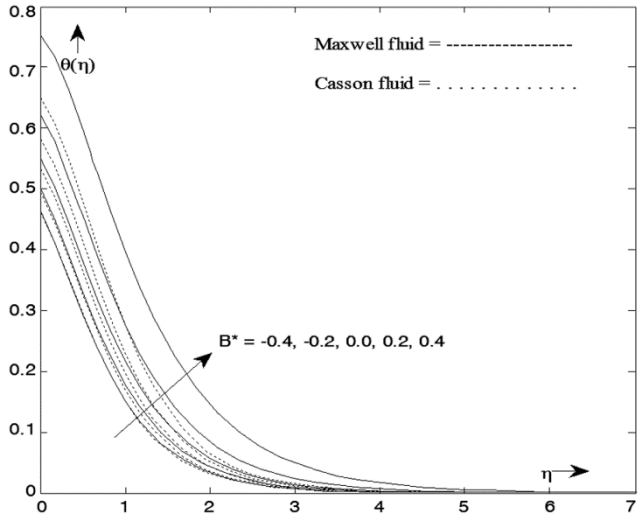

Fig. 15 — Effect of the temperature dependent heat source/sink parameter on temperature when
$K = 0.1, M = 1, A^* = 0.2, Sc = 0.7, k1 = 0.2, k2 = 0.1, Bi = 0.5,$
$Pr = 2.5, Ec = 0.1.$

temperature profile. Generally, non-negative values of the space dependent heat source/sink (A^*) performances as heat generators. Figures 16 and 17 indicate the influences of Prandtl and Eckert number on temperature profile. In Fig.16 enhancing value of Prandtl number diminishes the temperature distribution and thermal boundary layer thickness. Physically, rise in Prandtl number diminishes the thermal conductivity

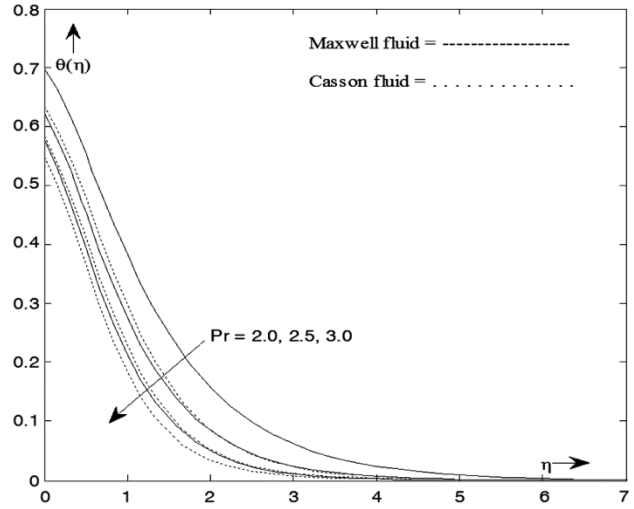

Fig. 16 — Effect of variation of the Prandtl number on temperature profile when

$K = 0.1, \mathrm{M} = 1, \mathrm{A}^* = 0.2, \mathrm{B}^* = 0.2, \mathrm{Sc} = 0.7, \mathrm{k1} = 0.2, \mathrm{k2} = 0.1, \mathrm{Bi} = 0.5, Ec = 0.1.$

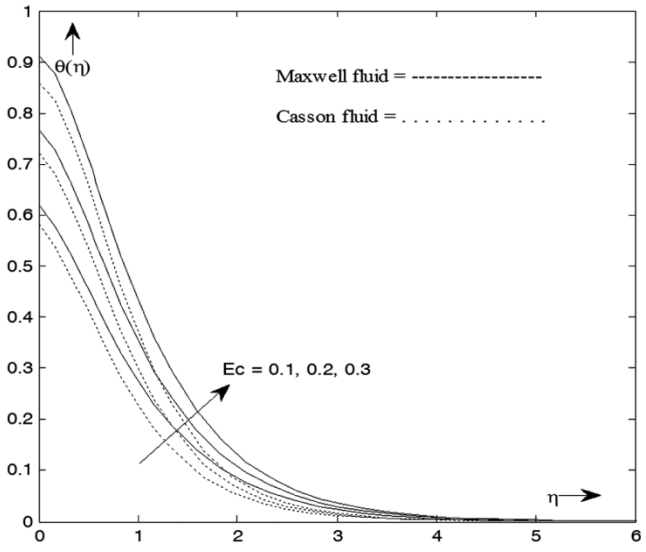

Fig. 17 — Effect of variation of the Eckert number on temperature profile when

$K = 0.1, \mathrm{M} = 1, \mathrm{A}^* = 0.2, \mathrm{B}^* = 0.2, \mathrm{Sc} = 0.7, \mathrm{k1} = 0.2, \mathrm{k2} = 0.1, \mathrm{Bi} = 0.5, \mathrm{Pr} = 2.5.$

of fluid consequently, thermal boundary layer thickness reduces. In Fig.17 high Eckert number denotes high heat level created by friction hence improved temperature on the system.

Figures 18 and 19 depicts that the impacts of Casson parameter and Maxwell fluid parameter on fluid temperature distribution. Casson parameter and Maxwell fluid parameter enhance with increasing value

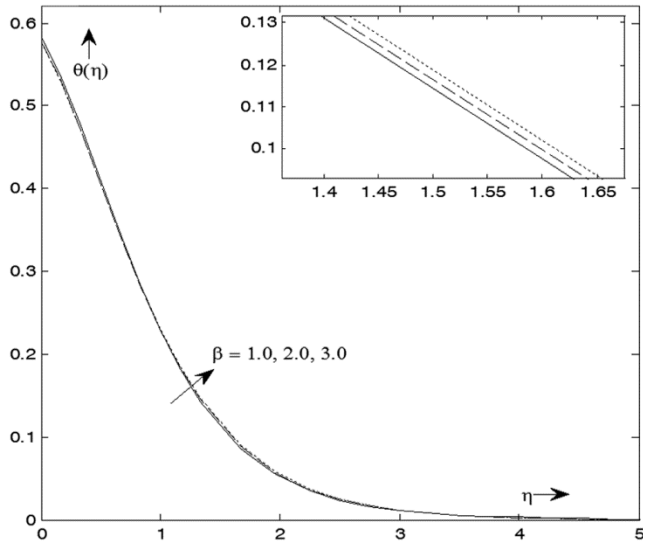

Fig. 18 — Effect of variation of the Casson parameter on temperature profile when

$K = 0.1, \delta_m = 0.5, \mathrm{M} = 1, \mathrm{A}^* = 0.2, \mathrm{B}^* = 0.2, \mathrm{Sc} = .7, \mathrm{k1} = 0.2, \mathrm{k2} = 0.1, \mathrm{Bi} = 0.5, \mathrm{Pr} = 2.5, Ec = 0.1.$

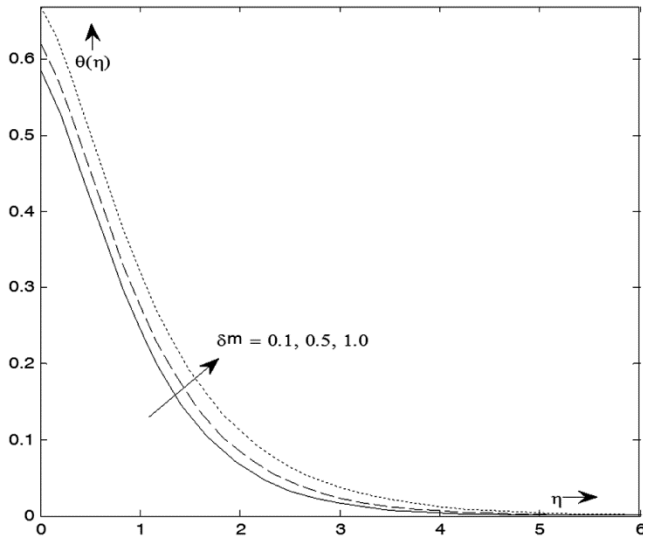

Fig. 19 — Effect of variation of the Maxwell parameter on temperature profile when

$K = 0.1, \mathrm{M} = 1, \beta = 1, \mathrm{A}^* = 0.2, \mathrm{B}^* = 0.2, \mathrm{Sc} = 0.7, \mathrm{k1} = 0.2, \mathrm{k2} = 0.1, \mathrm{Bi} = 0.5, \mathrm{Pr} = 2.5, Ec = 0.1.$

of temperature distribution. This induces an enhance in the absolute value of temperature gradient at surface. The trend of temperature gradient at surface with enhancing value of Casson parameter. Figure 20 displays the influence of Prandtl number on the entropy generation number. The entropy generation number enhances near the wall, but away from the wall reduces

with enhancing values of Prandtl number. The entropy generation number is higher for lower Prandtl number. Increasing values of the Prandtl number diminishes the fluid temperature. This sharp decrease of the temperature profiles leads to sharp decrease in the entropy generation number in the flow system.

The influence of the magnetic parameter on the entropy is shown in Fig. 21. The entropy generation number enhances near the wall, but away from the wall, diminishes with enhancing values of magnetic parameter. The entropy increases with the magnetic parameter. This happens because the magnetic field supports entropy in the fluid. Physically the presence of the magnetic field creates more entropy generation in the fluid as the fluid as fluid flow velocity is reduced. Figure 22 displays the influence of the dimensionless group parameter on the entropy. The relative significance of viscous consequence on the flow is determined by this parameter. In the figure, the entropy generation number is greater for high dimensionless group parameter. The fact that for higher dimensionless group parameter, the entropy due to fluid friction is enhanced. Figure 23 demonstrations the effect of the Eckert number on the entropy generation number. The entropy generation number enhances near the wall, but away from the wall diminishes with enhancing values of Eckert number. Viscous dissipation produces heat due to drag between the fluid particles, which causes an increase in fluid temperature, a positive Eckert number ($Ec > 0$) corresponds to fluid heating (heat is being supplied across the walls into the fluid) that means fluid is being heated.

Figures 24-26 show the consequence of space and temperature dependent heat source/sink parameter and Permeability parameter on entropy generation number. Space and temperature dependent heat

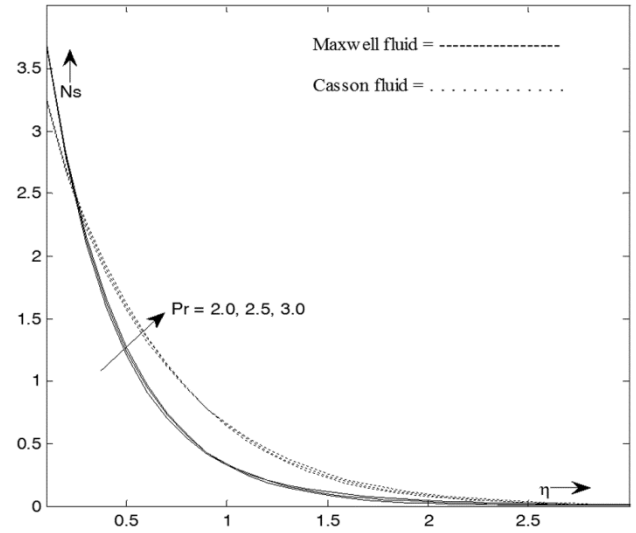

Fig. 20 — Effect of variation of the Prandtl number on entropy generation number when
$K = 0.1, \mathrm{M} = 1, \mathrm{A}^* = 0.2, \mathrm{B}^* = 0.2, \mathrm{Sc} = 0.7, \mathrm{k1} = 0.2, \mathrm{k2} = 0.1, \mathrm{Bi} = 0.5, Ec = 0.1, Br = 1, \Omega = 1, \mathrm{Re}_L = 1.$

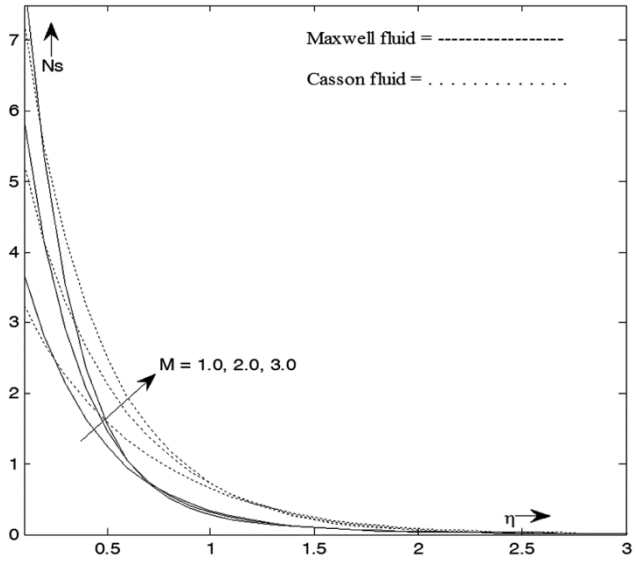

Fig. 21 — Effect of variation of the magnetic parameter on entropy generation number when
$K = 0.1, \mathrm{A}^* = 0.2, \mathrm{B}^* = 0.2, \mathrm{Sc} = .7, \mathrm{k1} = 0.2, \mathrm{k2} = 0.1, \mathrm{Bi} = 0.5, \mathrm{Pr} = 2.5, Ec = 0.1, Br = 1, \Omega = 1, \mathrm{Re}_L = 1.$

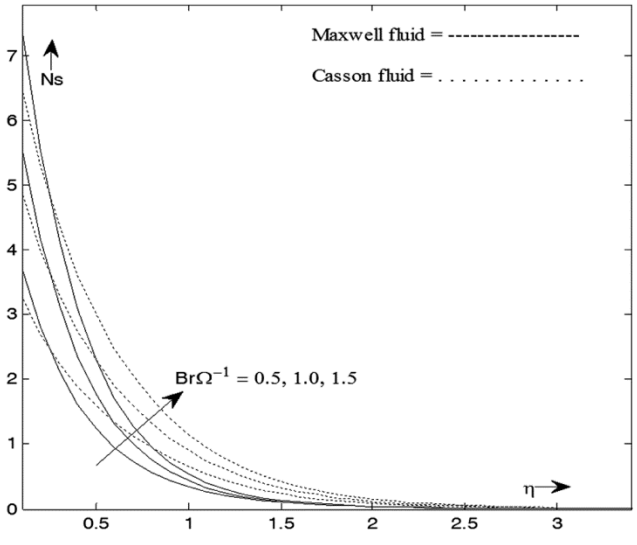

Fig. 22 — Effect of the dimensionless group parameter on entropy generation number when
$K = 0.1, \mathrm{M} = 1, \mathrm{A}^* = 0.2, \mathrm{B}^* = 0.2, \mathrm{Sc} = 0.7, \mathrm{k1} = 0.2, \mathrm{k2} = 0.1, \mathrm{Bi} = 0.5, \mathrm{Pr} = 2.5, Ec = 0.1, \mathrm{Re}_L = 1.$

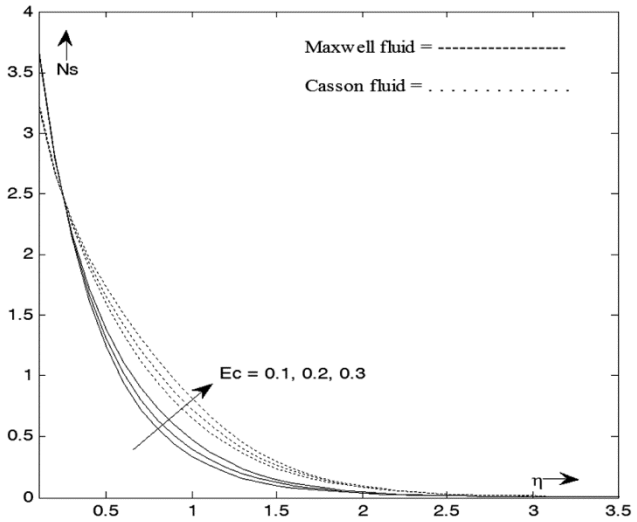

Fig. 23 — Effect of variation of the Eckert number on entropy generation number when
$K = 0.1, \mathrm{M} = 1, \mathrm{A}^* = 0.2, \mathrm{B}^* = 0.2, \mathrm{Sc} = 0.7, \mathrm{k1} = 0.2, \mathrm{k2} = 0.1, \mathrm{Bi} = 0.5, \mathrm{Pr} = 2.5, Br = 1, \Omega = 1, \mathrm{Re}_L = 1.$

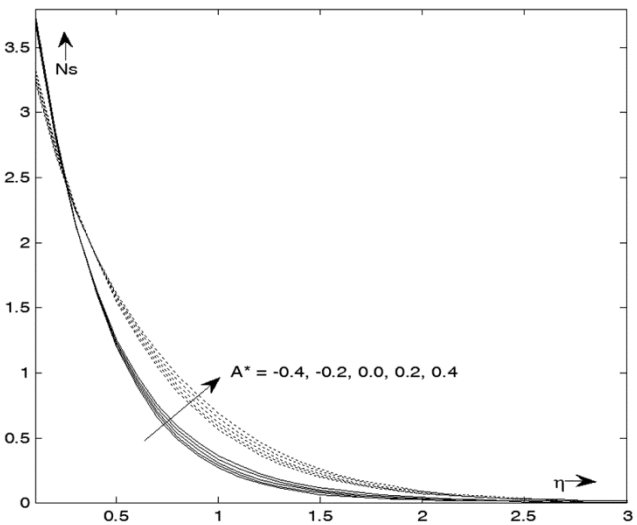

Fig. 24 — Effect of the space dependent heat source/sink parameter on entropy profile when
$K = 0.1, \mathrm{M} = 1, \mathrm{B}^* = 0.2, \mathrm{Sc} = 0.7, \mathrm{k1} = 0.2, \mathrm{k2} = 0.1, \mathrm{Bi} = 0.5, \mathrm{Pr} = 2.5, Ec = 0.1, Br = 1, \Omega = 1, \mathrm{Re}_L = 1.$

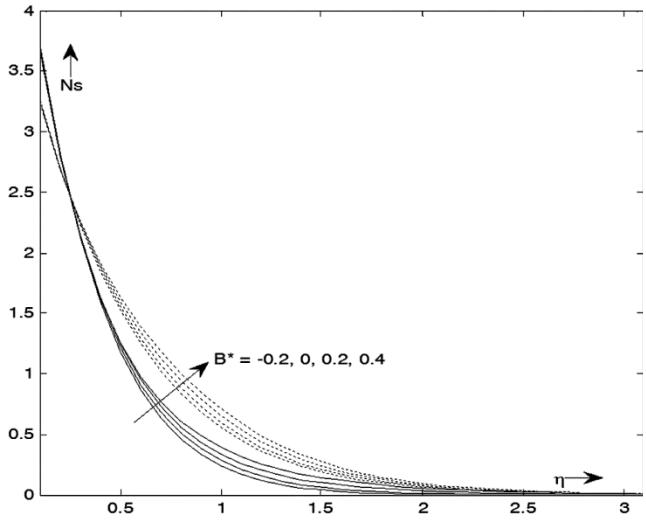

Fig. 25 — Effect of the temperature dependent heat source/sink parameter on entropy profile when
$K = 0.1, \mathrm{M} = 1, \mathrm{A}^* = 0.2, \mathrm{Sc} = 0.7, \mathrm{k1} = 0.2, \mathrm{k2} = 0.1, \mathrm{Bi} = 0.5, \mathrm{Pr} = 2.5, Ec = 0.1, Br = 1, \Omega = 1, \mathrm{Re}_L = 1.$

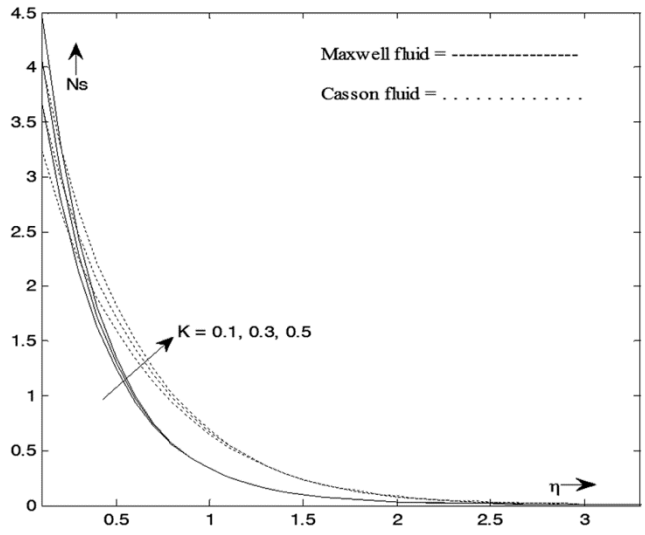

Fig. 26 — Effect of variation of the permeability parameter on entropy generation number when
$\mathrm{M} = 1, \mathrm{A}^* = 0.2, \mathrm{B}^* = 0.2, \mathrm{Sc} = 0.7, \mathrm{k1} = 0.2, \mathrm{k2} = 0.1, \mathrm{Bi} = 0.5, \mathrm{Pr} = 2.5, Ec = 0.1, Br = 1, \Omega = 1, \mathrm{Re}_L = 1.$

source/sink parameter and permeability parameter increases with the enhancing value of entropy generation number. Alternatively, declining the magnitude of the above parameters, achieves the main goal of the second law of thermodynamics, the minimizing of entropy generation. Figure 27 illustrates the effects of Biot number Bi on the entropy generation number. Near the stretching surface, the effects of Biot on entropy generation number are prominent. Increase in entropy generation number with an increase in the Biot number in the boundary layer region. In the region far away from the surface of the stretching sheet, the entropy generation is negligible. Therefore, the entropy can be minimized by increasing the convection through the boundary.

Figure 28 shows that the entropy increases with the increasing value of the Reynolds number. Reynolds number generates the higher entropy. Entropy function strongly depends upon Reynolds number. With high Reynolds number, hectic motion occurs because as Reynolds number increases, the fluid moves more disturbingly and thus the contribution of fluid friction and heat transfer on entropy result tends to rise in entropy generation. Figures 29-31 depicts the influence of Reynolds number, permeability parameter and dimensionless group parameter on the Bejan number. Permeability parameter rises near the wall, but away from the wall decreases with rising value of Bejan number. While the Reynolds number and dimensionless group parameter enhances with increasing value of Bejan number.

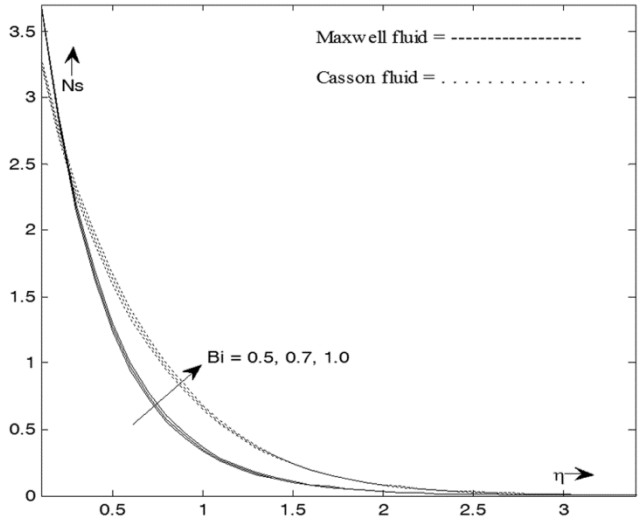

Fig. 27 — Effect of variation of the Biot number on entropy generation number when

$K = 0.1, \mathrm{M} = 1, \mathrm{A}^* = 0.2, \mathrm{B}^* = 0.2, \mathrm{Sc} = 0.7, \mathrm{k1} = 0.2, \mathrm{k2} = 0.1, \mathrm{Pr} = 2.5, Ec = 0.1, Br = 1, \Omega = 1, \mathrm{Re}_L = 1.$

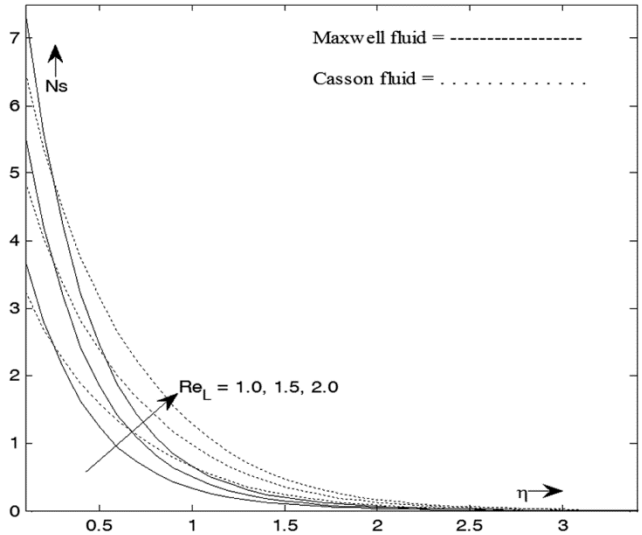

Fig. 28 — Effect of variation of the Reynolds number on entropy profile when

$K = 0.1, \mathrm{M} = 1, \mathrm{A}^* = 0.2, \mathrm{B}^* = 0.2, \mathrm{Sc} = 0.7, \mathrm{k1} = 0.2, \mathrm{k2} = 0.1, \mathrm{Pr} = 2.5, Ec = 0.1, Bi = 0.5, Br = 1, \Omega = 1.$

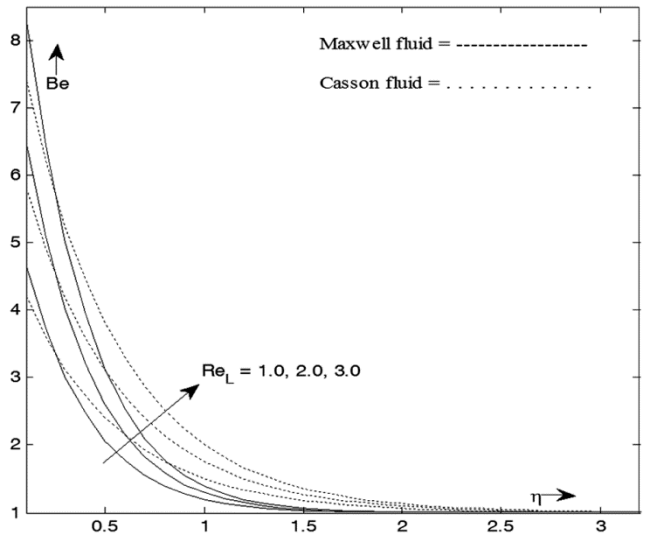

Fig. 29 — Effect of variation of the Reynolds number on Bejan number when

$K = 0.1, \mathrm{M} = 1, \mathrm{A}^* = 0.2, \mathrm{B}^* = 0.2, \mathrm{Sc} = 0.7, \mathrm{k1} = 0.2, \mathrm{k2} = 0.1, \mathrm{Pr} = 2.5, Ec = 0.1, Bi = 0.5, Br = 1, \Omega = 1.$

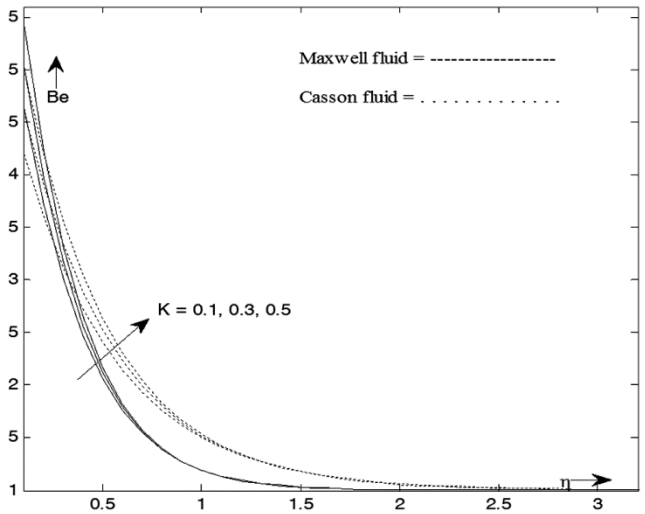

Fig. 30 — Effect of variation of the permeability parameter on Bejan number when

$\mathrm{M} = 1, \mathrm{A}^* = 0.2, \mathrm{B}^* = 0.2, \mathrm{Sc} = 0.7, \mathrm{k1} = 0.2, \mathrm{k2} = 0.1, \mathrm{Pr} = 2.5, Ec = 0.1, Bi = 0.5, Br = 1, \Omega = 1, \mathrm{Re}_L = 1.$

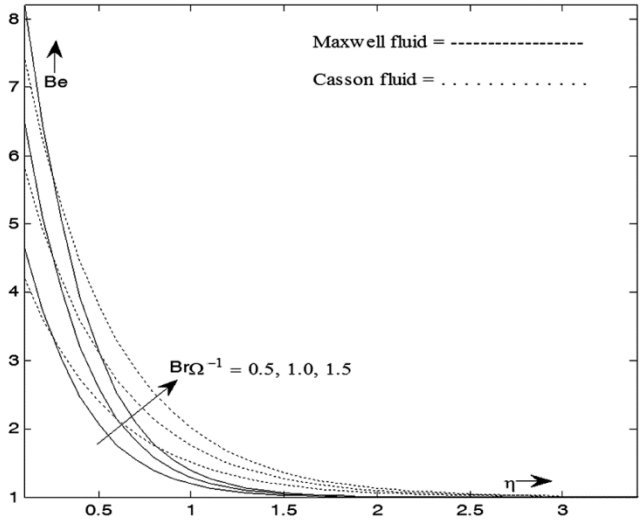

Fig. 31 — Effect of variation of the dimensionless group parameter on Bejan number when $K = 0.1, \mathrm{M} = 1, \mathrm{A}^* = 0.2, \mathrm{B}^* = 0.2, \mathrm{Sc} = 0.7, \mathrm{k1} = 0.2, \mathrm{k2} = 0.1, \mathrm{Pr} = 2.5, Ec = 0.1, Bi = 0.5, \mathrm{Re}_L = 1.$

7 Conclusions

The entropy analysis of non-Newtonian flow of Maxwell and Casson fluid over a permeable sheet with homogeneous and heterogeneous reaction with space and temperature dependent heat source/sink parameter has been investigated. The consequences of our investigation are summarized below:

(i) It is observed that boundary layer flow of viscoelastic fluid is highly affected by Lorentz force as compared with Casson fluid.

(ii) The impacts of Maxwell parameter, Casson parameter, magnetic parameter and porosity parameter decelerate the fluid velocity decrease.

(iii) Concentration profile reduces with enhancing values of magnetic parameter, permeability parameter, homogeneous and heterogeneous parameter, whereas Schmidt number presents reverse behavior.

(iv) Maxwell parameter, Casson parameter, Biot number, magnetic parameter, Eckert number, space and temperature dependent heat source/sink parameter and porosity parameter increase the temperature profile, whereas Prandtl number shows the reverse behavior.

(v) Reynolds number generates the higher entropy.

(vi) Entropy generation number and Bejan number rises with increasing value of dimensionless group parameter, Reynolds number and porosity parameter.

References

1 Kumaran G, Sandeep N & Ali M E, *Res Phys*, 7 (2017) 147.
2 Ramesh G K, Gireesha B J, Hayat T & Alseadi A, *Alex Eng J*, 55 (2016) 857.
3 Ramesh G K & Gireesha B J, *Ain Shams Eng J*, 5 (2014) 991.
4 Venkateswarlu B & Satya Narayan P V, *Front Heat Mass Trans*, 9 (2017) DOI: 10.5098.
5 Madhu M, Kishan N & Chamkha A J, *Propul Power Res*, 6 (2017) 31.
6 Mukhopadhyay S & Bhattacharya K, *J Egypt Math Soc*, 20 (2012) 229.
7 Aman S, Ilyas K, Ismail Z, Salleh M Z & Al-Mdallal Q M, *Scientific Reports,* 7 (2017) 2445.
8 Aman S, Khan I, Ismail Z & Salleh M Z, *J King Saud Univ Sci*, (2018).
9 Mahanthesh B, Gireesha B J, Shashikumar N S, Hayat T & Alseadi A, *Res Phys*, 9 (2018) 78.
10 Jain S & Choudhary R, *Int J Fluid Mech Res*, 45 (2018) 1.
11 Gopal D, Kishan N & Raju C S K, *Inform Med Unlocked*, 9 (2017) 154.
12 Raju C S K & Sandeep N, *Acta Astronautica*,133 (2017) 436.
13 Ullah I, Shafie S & Khan I*, J King Saud Univ Sci*, 29 (2017) 250.
14 Qayyum M, Khan H & Khan O, *Res Phys*, 7 (2017) 732.
15 Srinivas S, Kumar C K & Reddy A S, *Nonlinear Anal: Model*, 23 (2018) 213.
16 Yousif M A, Mahmood B A & Rashidi M M*, J Math Comput Sci*, 17 (2017) 169.
17 Ariel P D, Syam M I & Al-Mdallal Q M, *Int J Comput Math*, 90 (2013) 1990.
18 Ferdows M & Al-Mdallal Q M, *Am J Fluid Dynamics*, 2 (2012) 89.
19 Haque M M, Alam M M, Ferdows M & Al-Mdallal Q M, *Int J Appl Electromagn Mech*, 41 (2013) 121.
20 Merkin J H, *Math Comput Modell*, 24 (1996) 125.
21 Bachok N, Ishak A & Pop I, *Commun Nonlinear Sci Numer Simulat*, 16 (2011) 4296.
22 Kameswaran P K, Shaw S, Sibanda S & Murthy P V S N, *Int J Heat Mass Transfer*, 57 (2013) 465.
23 Malik M Y, Salahuddin T, Hussain A, Bilal S & Awais M, *AIP Advances*, 5 (2015) 107227.
24 Sheikh M & Abbas Z, *Ain Shams Eng J*, 8 (2017) 467.
25 Bejan A, *J Heat Transfer*, 101 (1979) 718.
26 hateyi S, Motsa S S & Makukula Z, *J Appl Fluid Mech*, 8 (2015) 21.
27 Ahmed S E, Mansour M A, Mahdy A & Mohamed S S, *Int J Eng Sci Tech*, 20 (2017) 1553.
28 Qing J, Bhatti M M, Abbas M A, Rashidi M M & Ali M E, *Entropy*, 18 (2016) 123.
29 Selvi R K, Muthuraj R & Srinivas S, *Global J Res Eng*, 18 (2018).
30 Qasim M, Khan Z H, Khan I & Al-Mdallal Q M, *Entropy*, 19 (2017) 490.
31 Bhatti M M, Abbas T & Rashidi M M*, J Magnetics*, 21 (2016) 468.
32 Jamalabadi M Y A, Hooshmand P, Bagheri N, Khakrah H & Dousti M, *Entropy,* 18 (2016) 147.
33 Srinivasacharya D & Bindu K H, *Alex Eng J*, 55, (2016) 973.
34 Jangili S, Gajjela N & Beg O N, *Alex Eng J*, 55 (2016) 1969.
35 Baag S, Mishra S R, Dash G C & Acharya M R, *Ain Shams Eng J*, 8 (2017) 623.

36 Rehman S U, Haq R U, Khan Z H & Lee C, *J Taiwan Inst Chem Eng*, 1 (2016).

37 Zhu Q Y, Zhuang Y J & Yu H Z, *Int J Heat Mass Trans*, 106 (2017) 61.

38 Srinivas J, Murthy J V R & Sai K S, *Comput Thermal Sci*, 7 (2015) 123.

39 Kareem S O, Adesanya S O & Vincent U E, *Alexandria Eng J*, 55 (2016) 925.

40 Khan N A, Naz F & Sultan F, *Open Eng*, 7 (2017) 185.

41 Jain S, Kumar V & Bohra S, *Int J Energy Technol*, 7 (2015) 40.

42 Naramgari S & Sulochana C, *Alex Eng J*, 55 (2016) 819.

43 Zaimi K, Ishak A & Pop I, *PLOS ONE*, 9 (2014) 1.

44 Chen C H, *Heat Mass Transfer*, 33 (1998) 471.